Inverse Problems for Inertial Sensor Calibration

David L. Olson

April 2, 2025

Contents

Abstract

Inertial sensors are vital to navigation, guidance, and control (NGC) for a variety of vehicles. Inertial sensors such as accelerometers and gyroscopes measure specific and angular velocity respectively which are mechanized to produce a position, velocity, and attitude (PVA) solution [1]. All inertial sensors are subject to deterministic and stochastic error which require careful calibration and characterization before utilizing inertial sensors in a vehicle application. In industry, the current state of the art for inertial sensor calibration has made little advancement over the past couple decades, where calibration data is collected and post-processed using basic statistics to compute basic error model parameters. In the past, improved fidelity for calibration required purchasing higher and higher precision equipment, which eventually succumbs to the law of diminishing returns.

However, ongoing research addressing inertial sensor calibration seeks to break dependence on high-cost high-precision test equipment by introducing advanced estimation techniques and stochastic filtering to maintain high fidelity calibration performance [2, 3, 4, 5, 6]. While various papers only tackle small pieces of an entire calibration procedure, there is an opportunity to cast inertial sensor calibration as an inverse problem to provide a holistic methodology to the field. The forward problem is simply the process of transforming true dynamic inputs acting on the sensor to sensor outputs which is subject to error. Then, the inverse problem takes the form of calibration in which calibration parameters are estimated from collected sensor data. Using inverse problem techniques, calibration parameter estimation can advance beyond basic statistical techniques for higher fidelity performance to include covariance propagation to assign confidence to final calibration parameters. In addition, estimation may be performed in real-time during the collection of calibration data, alleviating logistical and programmatic troubles for an inertial test laboratory.

The author plans to build upon previous work [7] which homogenized multiple IEEE standards for varying accelerometer and gyroscope technologies [8, 9, 10, 11, 12, 13, 14] which provide highly detailed inertial sensor error models. Inertial sensor data will be simulated using [15] which can provide true inertial sensor measurements which can then be corrupted with error and noise. Then, inverse problem techniques may be demonstrated and contrasted with traditional methods to showcase improvements and possible limitations to using these new highly detailed models. Higher fidelity calibration yields increased sensor accuracy, which ultimately enhances inertial navigation capabilities for a wide range of vehicle applications.

1 Introduction

A key challenge for self-driving cars is autonomous navigation. Autonomous navigation fuses the inputs of multiple sensors to formulate a position, velocity, and attitude (PVA) solution for the vehicle of interest. Common navigation sensors include inertial measurement units (IMUs), global positioning system (GPS) receivers, odometers, magnetometers, radars, LiDAR, cameras, and many others. It is crucial to not only formulate a navigation solution but also to track the uncertainty of that solution, which can play an important role in decision-making and risk-assessment for autonomous self-driving vehicle applications.

IMUs generally contain three accelerometers and gyroscopes pointing in all three Cartesian axes which measure specific force and angular velocity respectively. These measurements are integrated to provide a PVA solution, but an IMU-only solution will drift away from truth unbounded due to the integration of sensor noise and other errors [1]. An inertial navigation system (INS) integrates the IMU measurements and then uses GPS to provide accurate measurements of position to fuse with the IMU solution typically via a Kalman filter thus combating any position error drift. This allows for long-term accurate navigation suitable for a self-driving car traveling long distances.

A driving need for navigation regarding self-driving cars is forming back-up modes of navigation when GPS signals are temporarily unavailable. This is especially important in urban environments where tall buildings and tunnels can cause signal blockages. Lack of GPS signals are problematic for an INS as its performance is dependent on receiving those signals, and the IMU-only solutions will drift away quickly from ground truth. Inertial-only navigation is suitable for short periods such as temporary GPS signal blockages, but the duration of a suitable inertial-only navigation is highly dependent on the quality of sensors contained within an IMU. This dilemma, among any others, motivates the need for rigorous IMU calibration and compensation.

One particular challenge with the use of commercial-grade or automotive-grade micro-electrical mechanical system (MEMS) inertial sensors is their sensitivity to temperature. Characterizing how common error sources such as bias, scale factors, and misalignments shift in response to temperature is a tough problem which requires hours of testing per unit and is often too burdensome for applications using automotive-grade devices.

1.1 Defining Sensor Error

Accelerometers and gyroscopes are subject to a variety of error sources such as biases, scale factor imperfections, axis misalignments, noise, and many others. IMU calibration is the process of characterizing these error sources, while compensation is the process of correcting measurements in real-time to provide the most accurate and precise measurements possible. The better these error sources are characterized, the slower that the IMU-only navigation solution will drift away from truth.

Inertial sensor calibration can be treated as an inverse problem. Consider an accelerometer as an example where the ideal forward model is quite straight forward; specific force in equals specific force out. Unfortunately in practice, we are not quite so lucky. Any error in the forward model is defined as

$$\Delta f := \tilde{f} - f$$

where Δf is the measurement error, $\tilde{f}$ is the specific force measured by the sensor which is

subject to error, and f is the true specific force acting on the accelerometer. The same applies to gyroscope measurements.

$$\Delta\omega := \tilde{\omega} - \omega$$

Inertial sensor errors Δf and $\Delta\omega$ are subject to both deterministic and stochastic error and any number of contributing factors can make up these terms.

There are many procedures available to calibrate inertial sensors such as [2] which require high-precision equipment to point and spin inertial sensors at known directions or quantities to separate measurement truth from measurement error.

1.1.1 Basic IMU Error Sources and Error Models

Consider an IMU which contains three accelerometers and three gyroscopes arranged to point in a standard Cartesian right-handed coordinate frame. A basic forward model framework appropriate for commercial- and automotive-grade inertial sensors is provided in [1].

$$\begin{aligned} \tilde{\boldsymbol{f}} &= [I + M_a]\,\boldsymbol{f} + \boldsymbol{b}_a + \boldsymbol{w}_a, \quad \boldsymbol{w}_a \sim N\left(0, \sigma^2\right) \\ \tilde{\boldsymbol{\omega}} &= [I + M_g]\,\boldsymbol{\omega} + \boldsymbol{b}_g + \boldsymbol{w}_g \quad \boldsymbol{w}_g \sim N\left(0, \sigma^2\right) \end{aligned} \tag{1}$$

In these models are bias terms $\boldsymbol{b}_a$, $\boldsymbol{b}_g \in \mathbb{R}^3$ for the accelerometers and gyroscopes respectively. In addition are the misalignment matrices M_a, $M_g \in \mathbb{R}^{3\times3}$, whose diagonal elements are scale factor error terms. The off-diagonal elements are misalignment terms which account for imperfections in the alignment of the sensing axes. All inertial sensors are also subject to noise, which is captured by terms $\boldsymbol{w}_a$, $\boldsymbol{w}_g$ which are additive zero-mean white Gaussian noise. Equation 2 restates equation 1 in terms of all its various elements.

$$\begin{aligned} \begin{bmatrix} \tilde{f}_x \\ \tilde{f}_y \\ \tilde{f}_z \end{bmatrix} &= \begin{bmatrix} 1+s_{a,x} & m_{a,xy} & m_{a,xz} \\ m_{a,yx} & 1+s_{a,y} & m_{a,yz} \\ m_{a,zx} & m_{a,zy} & 1+s_{a,z} \end{bmatrix} \begin{bmatrix} f_x \\ f_y \\ f_z \end{bmatrix} + \begin{bmatrix} b_{a,x} \\ b_{a,y} \\ b_{a,z} \end{bmatrix} + \begin{bmatrix} w_{a,x} \\ w_{a,y} \\ w_{a,z} \end{bmatrix} \\ \begin{bmatrix} \tilde{\omega}_x \\ \tilde{\omega}_y \\ \tilde{\omega}_z \end{bmatrix} &= \begin{bmatrix} 1+s_{g,x} & m_{g,xy} & m_{g,xz} \\ m_{g,yx} & 1+s_{g,y} & m_{g,yz} \\ m_{g,zx} & m_{g,zy} & 1+s_{g,z} \end{bmatrix} \begin{bmatrix} \omega_x \\ \omega_y \\ \omega_z \end{bmatrix} + \begin{bmatrix} b_{g,x} \\ b_{g,y} \\ b_{g,z} \end{bmatrix} + \begin{bmatrix} w_{g,x} \\ w_{g,y} \\ w_{g,z} \end{bmatrix} \end{aligned} \tag{2}$$

The goal of IMU calibration is characterize to these IMU error sources, resulting in estimates $\hat{\boldsymbol{b}}_a$, $\hat{M}_a$, $\hat{\boldsymbol{b}}_g$, $\hat{M}_g$ which then allows for the correction of inertial sensor measurements in real-time, which is referred to as compensation. In essence, this can be treated as the inverse model with estimated parameters. Using the estimated model parameters, inertial sensor measurements $\tilde{\boldsymbol{f}}$, $\tilde{\boldsymbol{\omega}}$ are compensated to provide new measurements $\hat{\boldsymbol{f}}$, $\hat{\boldsymbol{\omega}}$ per equation 3.

$$\hat{\boldsymbol{f}} = \left[I + \hat{M}_a\right]^{-1}\left(\tilde{\boldsymbol{f}} - \hat{\boldsymbol{b}}_a\right)$$

$$\hat{\boldsymbol{\omega}} = \left[I + \hat{M}_g\right]^{-1} \left(\tilde{\boldsymbol{\omega}} - \hat{\boldsymbol{b}}_g\right) \tag{3}$$

1.1.2 Traditional Inertial Sensor Calibration

IMUs are traditionally calibrated on some sort of a rotational test bed. These rotation test beds are able to point and spin inertial sensors at known quantities with sharp precision. To calibrate accelerometers, the IMU is aligned in various poses along the local gravity vector at that location, therefore a gravity survey within an inertial test laboratory is critical. To calibrate gyroscopes, the IMU is spun at known speeds.

For example hardware, consider the 2103C Series Three-Axis Position and Rate Table System from Ideal Aerosmith shown in figure 1.

Figure 1: 2103C Series Three Axis Position and Rate Table System

Traditional calibration comprises of twelve tests with six for the accelerometers and six for the gyroscopes. In each test, the IMU is stationary for accelerometer tests and spinning at a constant speed for gyroscope tests. Each test is completed for a set amount of time, usually 60 seconds, and the measurements are averaged. Table 1 lists the six tests as well as the quantity for each averaged test result.

Accelerometer Tests	Gyroscope Tests
• Point X-Axis Up $\left(\bar{\boldsymbol{f}}^{+\mathrm{x}}\right)$ • Point X-Axis Down $\left(\bar{\boldsymbol{f}}^{-\mathrm{x}}\right)$ • Point Y-Axis Up $\left(\bar{\boldsymbol{f}}^{+\mathrm{y}}\right)$ • Point Y-Axis Down $\left(\bar{\boldsymbol{f}}^{-\mathrm{y}}\right)$ • Point Z-Axis Up $\left(\bar{\boldsymbol{f}}^{+\mathrm{z}}\right)$ • Point Z-Axis Down $\left(\bar{\boldsymbol{f}}^{-\mathrm{z}}\right)$	• Positive Spin about X-Axis $(\bar{\boldsymbol{\omega}}^{+\mathrm{x}})$ • Negative Spin about X-Axis $(\bar{\boldsymbol{\omega}}^{-\mathrm{x}})$ • Positive Spin about Y-Axis $(\bar{\boldsymbol{\omega}}^{+\mathrm{y}})$ • Negative Spin about Y-Axis $(\bar{\boldsymbol{\omega}}^{-\mathrm{y}})$ • Positive Spin about Z-Axis $(\bar{\boldsymbol{\omega}}^{+\mathrm{z}})$ • Negative Spin about Z-Axis $(\bar{\boldsymbol{\omega}}^{-\mathrm{z}})$

Table 1: Traditional IMU Calibration Tests

As an example from equation 2, the accelerometer bias $\boldsymbol{b}_a$ can be solved from the collected test data.

$$\boldsymbol{b}_a = \begin{bmatrix} b_{a,x} \\ b_{a,y} \\ b_{a,z} \end{bmatrix} = \frac{1}{2} \begin{bmatrix} \bar{f}_x^{+\mathrm{x}} + \bar{f}_x^{-\mathrm{x}} \\ \bar{f}_y^{+\mathrm{y}} + \bar{f}_y^{-\mathrm{y}} \\ \bar{f}_z^{+\mathrm{z}} + \bar{f}_z^{-\mathrm{z}} \end{bmatrix} \tag{4}$$

All model in parameters in equation 2 can be solved in a similar manner, which have all been listed in section 6.1.

1.2 Beyond Traditional IMU Calibration

While traditional calibration methods have proven successful over the past several decades, there is a push within the navigation community to move to systematic calibration methods [16]. It is difficult to estimate more model parameters with the same limited dynamics, and the piece-meal approach to post-processing IMU calibration data is cumbersome and complicated. Additionally, traditional means of calibration do not provide any sort of measure of uncertainty which many navigation algorithms, i.e., Kalman filters, require for any sort of state estimation.

Therefore, this paper aims to investigate systematic IMU calibration through the lens of inverse problem techniques. Come back here and tell everyone what you ended up doing.

2 Methods

Consider an IMU under test strapped down to a three axis rotational test bed. The rotational test bed provides measurements of angular position and angular rate along each test axis. As exemplar hardware, the unit under test will be a STIM 300 IMU from Safran and the 210C Series Three Axis Position and Rate Table System from Ideal Aerosmith.

2.1 STIM 300 IMU Specifications

The STIM 300 IMU, henceforth referred to as the unit under test (UUT), provides measurements of specific force and angular velocity. While the true forward model is unknown, it will be assumed that the basic forward model in equation 1 will sufficiently model the error of the device. Assuming the UUT uses the "10g" variant of accelerometers, bounds for the accelerometer-related model parameters are provided in table 5-5 of the specification sheet [17].

- Bias: $|b_a| \leq 7.5 \times 10^{-3} g$
- Scale Factor Error : $|s_a| \leq 200\,\text{ppm}$
- Misalignment: $|m_a| \leq 1 \times 10^{-3}\,\text{rad}$

The accelerometers are also subject to zero-mean Gaussian noise with a velocity random walk (VRW) value of $0.07\text{m/s}/\sqrt{\text{Hz}}$, which translates to a $\sigma_a = \frac{0.07}{60} = 0.0012\text{m}\,\text{s}^{-1}$. Likewise, [17] provides bounds for the gyroscopes in table 5-3.

- Bias: $|b_g| \leq 250^\circ\,\text{h}^{-1}$
- Scale Factor Error : $|s_g| \leq 500\,\text{ppm}$
- Misalignment: $|m_g| \leq 1 \times 10^{-3}\,\text{rad}$

The gyroscopes are also subject to zero-mean Gaussian noise with an angle random walk (ARW) value of $0.15^\circ/\sqrt{\text{h}}$ which translates to a $\sigma_g = \frac{0.15}{60}\frac{\pi}{180} = 4.3633 \times 10^{-5}\text{rad}\,\text{s}^{-1}$.

For simulation purposes, true model parameters will be selected within these bounds in later sections.

2.2 Formulating IMU Calibration as a Discrete Linear Inverse Problem

Recall the system of equations from equation 2 and consider the x-axis accelerometer measurements.

$$\tilde{f}_x = (1 + s_{a,x})\, f_x + m_{a,xy} f_y + m_{a,xz} f_z + b_{a,x}$$

The equation above can be re-arranged to express the model parameters as a function of the accelerometer error $\Delta f = \tilde{f} - f$.

$$\tilde{f}_x = (1 + s_{a,x})\, f_x + m_{a,xy} f_y + m_{a,xz} f_z + b_{a,x}$$

$$\tilde{f}_x - f_x = b_{a,x} + s_{a,x} f_x + m_{a,xy} f_y + m_{a,xz} f_z$$

$$\Delta f_x = b_{a,x} + s_{a,x} f_x + m_{a,xy} f_y + m_{a,xz} f_z$$

Assuming that both the UUT and test bed are able to provide synchronized measurements at the same sampling frequency, a series of measurements from these devices can be organized into another system of equations.

$$\begin{bmatrix} 1 & f_x[1] & f_y[1] & f_z[1] \\ 1 & f_x[2] & f_y[2] & f_z[2] \\ \vdots & \vdots & \vdots & \vdots \\ 1 & f_x[m] & f_y[m] & f_z[m] \end{bmatrix} \begin{bmatrix} b_{a,x} \\ s_{a,x} \\ m_{a,xy} \\ m_{a,xz} \end{bmatrix} = \begin{bmatrix} \Delta f_x[1] \\ \Delta f_x[2] \\ \vdots \\ \Delta f_x[m] \end{bmatrix} \tag{5}$$

This system of equations can be expressed in the form $G\boldsymbol{m} = \boldsymbol{d}$. In this expression, "true" measurements $f_x[n]$, $f_y[n]$, $f_z[n]$ within the model operator are computed from measurements provided by the test bed, and the model parameters are various calibration factors from the forward model. Elements of the data vector $\boldsymbol{d}$ are the difference of the UUT output and test bed output such that $d[n] = \tilde{f}_x[n] - f_x[n]$.

Let F be the model operator demonstrated by equation 5.

$$F := \begin{bmatrix} 1 & f_x[1] & f_y[1] & f_z[1] \\ 1 & f_x[2] & f_y[2] & f_z[2] \\ \vdots & \vdots & \vdots & \vdots \\ 1 & f_x[m] & f_y[m] & f_z[m] \end{bmatrix}, \quad F \in \mathbb{R}^{m \times 4} \tag{6}$$

Then, the discrete linear inverse problem for all accelerometer calibration parameters given in equation 2 can defined below.

$$G_a \boldsymbol{m}_a = \boldsymbol{d}_a \tag{7}$$

$$\begin{bmatrix} F & 0_{m\times 4} & 0_{m\times 4} \\ 0_{m\times 4} & F & 0_{m\times 4} \\ 0_{m\times 4} & 0_{m\times 4} & F \end{bmatrix} \begin{bmatrix} b_{a,x} \\ s_{a,x} \\ m_{a,xy} \\ m_{a,xz} \\ b_{a,y} \\ m_{a,yz} \\ s_{a,y} \\ m_{a,yz} \\ b_{a,z} \\ m_{a,zx} \\ m_{a,zy} \\ s_{a,z} \end{bmatrix} = \begin{bmatrix} \Delta f_x[1] \\ \vdots \\ \Delta f_x[m] \\ \Delta f_y[1] \\ \vdots \\ \Delta f_y[m] \\ \Delta f_z[1] \\ \vdots \\ \Delta f_z[m] \end{bmatrix}$$

Likewise, let Ω be the model operator for all gyroscope measurements specific to one sensor.

$$\Omega := \begin{bmatrix} 1 & \omega_x[1] & \omega_y[1] & \omega_z[1] \\ 1 & \omega_x[2] & \omega_y[2] & \omega_z[2] \\ \vdots & \vdots & \vdots & \vdots \\ 1 & \omega_x[m] & \omega_y[m] & \omega_z[m] \end{bmatrix}, \quad \Omega \in \mathbb{R}^{m \times 4} \tag{8}$$

Then, the discrete linear inverse problem for all gyroscope calibration parameters given in equation 2 can defined below.

$$G_g \boldsymbol{m}_g = \boldsymbol{d}_g \tag{9}$$

$$\begin{bmatrix} \Omega & 0_{m\times 4} & 0_{m\times 4} \\ 0_{m\times 4} & \Omega & 0_{m\times 4} \\ 0_{m\times 4} & 0_{m\times 4} & \Omega \end{bmatrix} \begin{bmatrix} b_{g,x} \\ s_{g,x} \\ m_{g,xy} \\ m_{g,xz} \\ b_{g,y} \\ m_{g,yz} \\ s_{g,y} \\ m_{g,yz} \\ b_{g,z} \\ m_{g,zx} \\ m_{g,zy} \\ s_{g,z} \end{bmatrix} = \begin{bmatrix} \Delta\omega_x[1] \\ \vdots \\ \Delta\omega_x[m] \\ \\ \Delta\omega_y[1] \\ \vdots \\ \Delta\omega_y[m] \\ \\ \Delta\omega_z[1] \\ \vdots \\ \Delta\omega_z[m] \end{bmatrix}$$

2.3 Model Covariance and Weighted Least Squares

As previously mentioned, one major benefit of systematic calibration vs. traditional calibration is the ability to produce some measure of uncertainty with respect to the estimated calibration model parameters. Given that inertial sensors are provided some terms within their specification sheets to determine a zero-mean Gaussian distribution for sensor noise, each discrete linear inverse problems formulated in the previous section can be reweighted to form weighted least squares problems. This provides an opportunity to examine how well the calibration model parameters fit the collected data by performing a χ^2 test and examining the resulting p-values.

For example, consider the system of equations for the accelerometer calibration parameters defined in equation 7. Recall, the standard deviation for accelerometer sensor noise is provided in section 2.1. This system of equations can be reweighted accordingly below.

$$W = \sigma_a I$$

$$W G_a \boldsymbol{m}_a = W \boldsymbol{d}_a \tag{10}$$

$$G_{a,w}\boldsymbol{m}_a = \boldsymbol{d}_{a,w}$$

The model covariance matrix for the accelerometer parameters is given in equation 11.

$$\text{Cov}\left(\boldsymbol{m}_{L2}\right) = \left(G_{a,w}^T G_{a,w}\right)^{-1} \tag{11}$$

From this, the 95% confidence bounds for the L2 regression solution $\boldsymbol{m}_{L2}$ are given below.

$$\boldsymbol{m}_{L2} \pm 1.96\text{diag}\left(\text{Cov}\left(\boldsymbol{m}_{L2}\right)\right)^{\frac{1}{2}} \tag{12}$$

Additionally, the χ^2 test may be formed to compute a p-value, allowing for another quantitative measure to determine how well the model fits the provided data. The χ^2 statistic is formed according to equation 13.

$$\chi^2_{\text{obs}} = \sum_i^m \frac{\left(d_i - \left(G\boldsymbol{m}_{L2}\right)_i\right)^2}{\sigma_i^2} \tag{13}$$

2.4 Simulating Calibration Data and Model Parameters

Rotational motion on the test bed will be simulated by developing a true sequence of angular velocities $\boldsymbol{\omega}$ across time t experienced by the UUT. The attitude of the UUT, represented by the direction cosine matrix $C\left(t\right)$, will be integrated in discrete steps such that the k^{th} step in the sequence is

$$C\left(t_k\right) = C_0 \prod_{i=1}^{k} e^{\left[\boldsymbol{\omega}\left(t_i\right)\times\right]\Delta t} \tag{14}$$

where $\left[\boldsymbol{\omega}\left(t_i\right)\times\right]$ is a skew-symmetric matrix and Δt is the time step. While the test bed rotates, the accelerometers will each be measuring components of the normal force from the test bed resulting from the acceleration due to gravity g. For each time step k, the true specific force quantity is given below.

$$\boldsymbol{f}\left(t_k\right) = C\left(t_k\right)\begin{bmatrix}0\\0\\g\end{bmatrix} \tag{15}$$

In the simulation, it will be assumed that quantities $\boldsymbol{\omega}$ and $\boldsymbol{f}$ will be available through measurement outputs of the test bed itself. Measurements of these quantities from the UUT will be corrupted with measurement error according to equations 2. The values of the model parameters are recorded in table 2 and are selected with reasonable orders of magnitude as discussed in section 2.1.

Model Parameter	Accel Value	Gyro Value
Fixed Bias X	$0\,\mathrm{m\,s^{-2}}$	$0\,\mathrm{rad\,s^{-1}}$
Fixed Bias Y	$0\,\mathrm{m\,s^{-2}}$	$0\,\mathrm{rad\,s^{-1}}$
Fixed Bias Z	$0\,\mathrm{m\,s^{-2}}$	$0\,\mathrm{rad\,s^{-1}}$
Scale Factor Error X	0 ppm	0 ppm
Scale Factor Error Y	0 ppm	0 ppm
Scale Factor Error Z	0 ppm	0 ppm
Misalignment XY	0 mrad	0 mrad
Misalignment XZ	0 mrad	0 mrad
Misalignment YX	0 mrad	0 mrad
Misalignment YZ	0 mrad	0 mrad
Misalignment ZX	0 mrad	0 mrad
Misalignment ZY	0 mrad	0 mrad

Table 2: UUT Simulated Model Parameters

Capabilities for simulating calibration sequences on test beds and IMU error models have been developed in MATLAB ® .

2.5 Experiment Design

Three calibration sequences will be considered for the application of inverse problem techniques to IMU calibration.

1. Traditional Calibration Sequence
2. Single-Axis Motion Calibration Sequence
3. Multi-Axis Motion Calibration Sequence

Each calibration sequence is intended to provide significant changes to the model operator which will then require consideration of how to solve the inverse problem. The following section will cover the results of each simulated experiment.

3 Results

3.1 Traditional Calibration Sequence

A traditional calibration sequence was simulated for a UUT with an assumed sample rate of 100 Hz. Each test specified in table 1 for a duration of 10 s. All of the accelerometer test data were appended together to build the model operator G_a, and as well as all of the gyroscope test data to build G_g. Before proceeding with solving for the weighted least squares solution, a quick check was performed to ensure the both G_a and G_g were full rank.

$$\begin{aligned} \text{rank}\,(G_a) &= 6, \;\; G_a \in \mathbb{R}^{60006\times 12} \\ \text{rank}\,(G_g) &= 6, \;\; G_g \in \mathbb{R}^{60006\times 12} \end{aligned} \tag{16}$$

The fact that both G_a and G_g are not full rank was not initially expected. However, given that the number of observations $m = 60006$ actually has many repeated rows as the UUT itself undergoes no changes in specific force and angular rate, this should not have been as much of a surprise. Instead of proceeding with solving for a solution, another calibration sequence was designed.

3.2 Single-Axis Motion Calibration Sequence

In response to the lack of full rank in the previous experiment design, a new calibration sequence was designed to put axis of the UUT in motion in hopes of establishing model operators of full rank. Figures 2 and 3 show the designed motion profile.

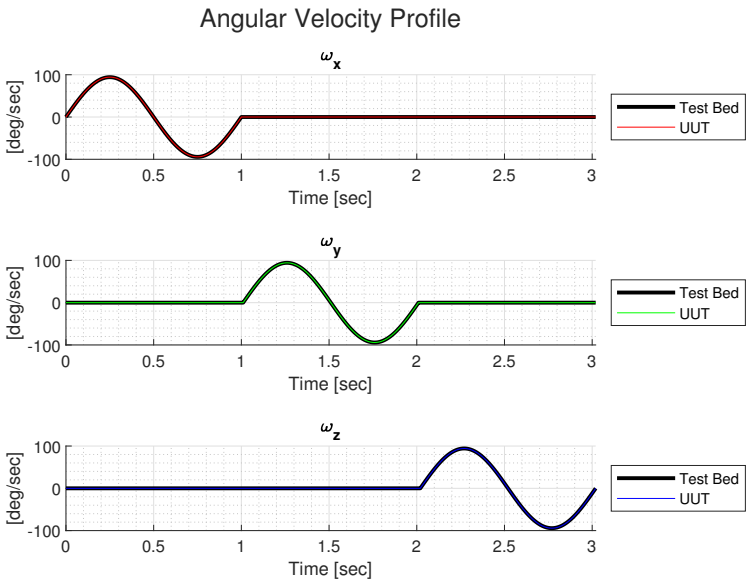

Figure 2: Single-Axis Angular Velocity Profile

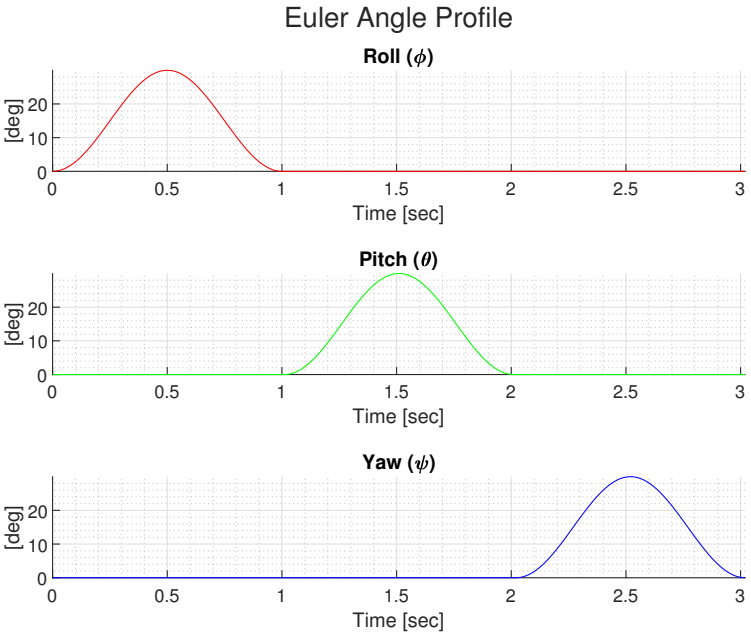

Figure 3: Single-Axis Euler Angle Profile

Due to the rotations of the test bed, the specific force is also altered as shown in figure 4.

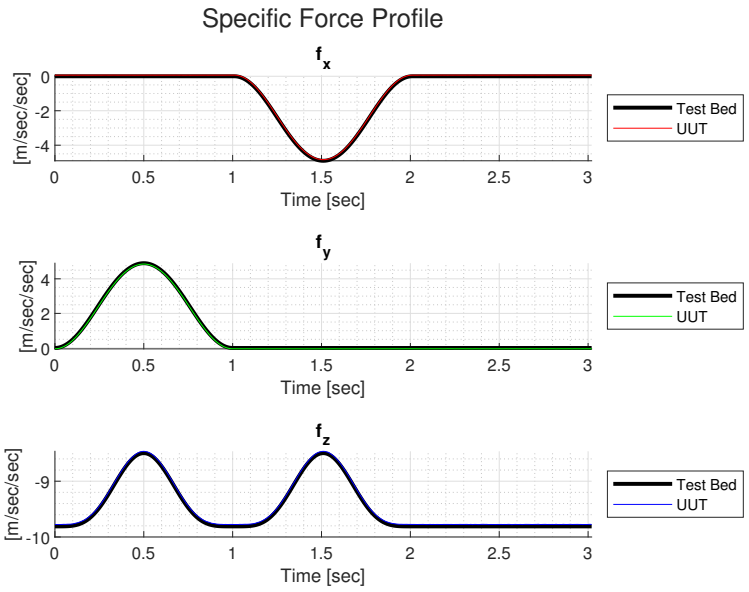

Figure 4: Single-Axis Specific Force Profile

3.2.1 Model Operator Rank

Even with new motion profiles, both model operators G_a and G_g are not full rank.

$$\begin{aligned} \text{rank}\,(G_a) = 12, \;\; G_a \in \mathbb{R}^{909\times 12} \\ \text{rank}\,(G_g) = 12, \;\; G_g \in \mathbb{R}^{909\times 12} \end{aligned} \tag{17}$$

In response, a model solution was still obtained using the generalized inverse. This rank-deficiency is of the type "$p = n$ and $p < m$, in which the data null space is non-trivial but the model null space is trivial. This implies that the solution will be unique, but cannot fit the general data exactly. For both G_a and G_g, a singular value decomposition (SVD) was performed and each decomposed matrix was truncated to the rank of the matrix. The generalized inverse model was formed accordingly below.

$$\begin{aligned} \boldsymbol{m}^a_\dagger = V_{a,p} S^{-1}_{a,p} U^T_{a,p} \boldsymbol{d}_a \\ \boldsymbol{m}^g_\dagger = V_{g,p} S^{-1}_{g,p} U^T_{g,p} \boldsymbol{d}_g \end{aligned} \tag{18}$$

Each model resolution matrix $R_m = V_p V_p^T$ shows that each model parameter has perfect resolution. The singular values for each model operator are shown in figures 5 and 6.

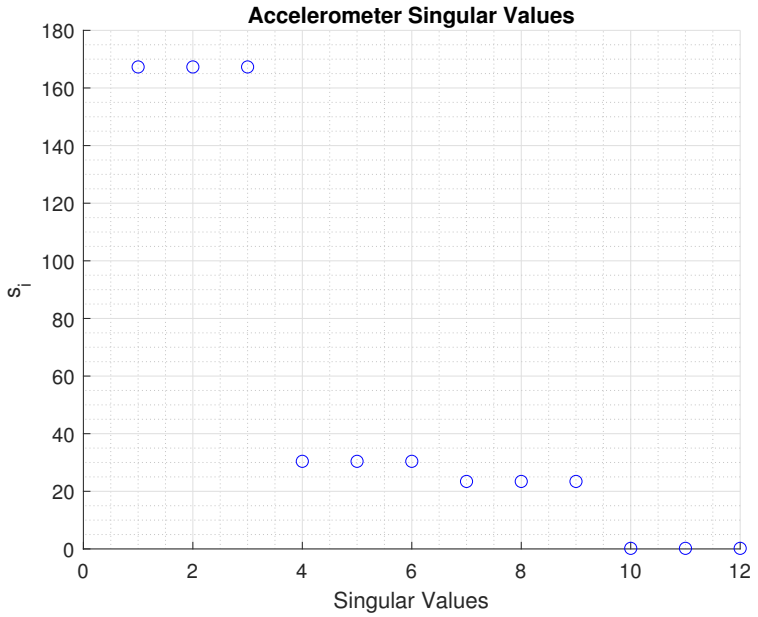

Figure 5: Accelerometer Singular Values

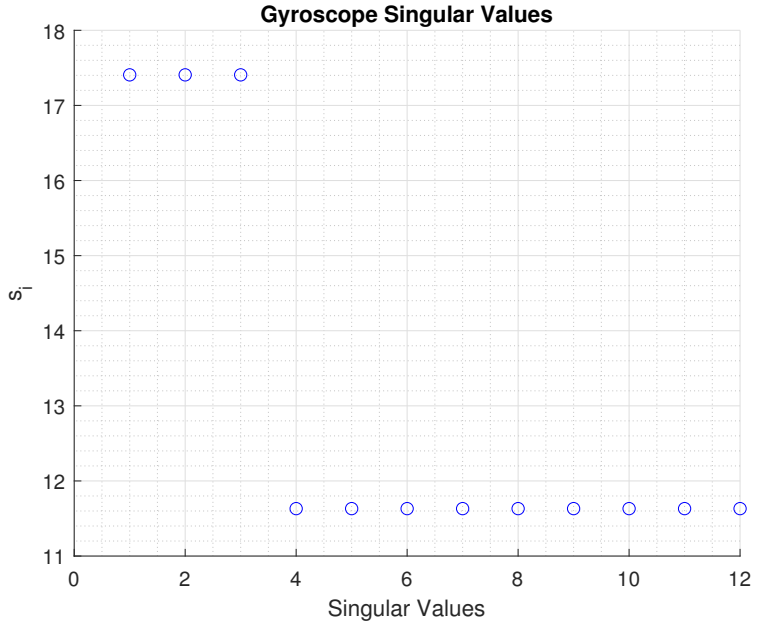

Figure 6: Gyroscope Singular Values

3.2.2 Estimated Model Parameters

The estimated model parameters and their associated errors are provided in figures 7, 8, 9, and 10.

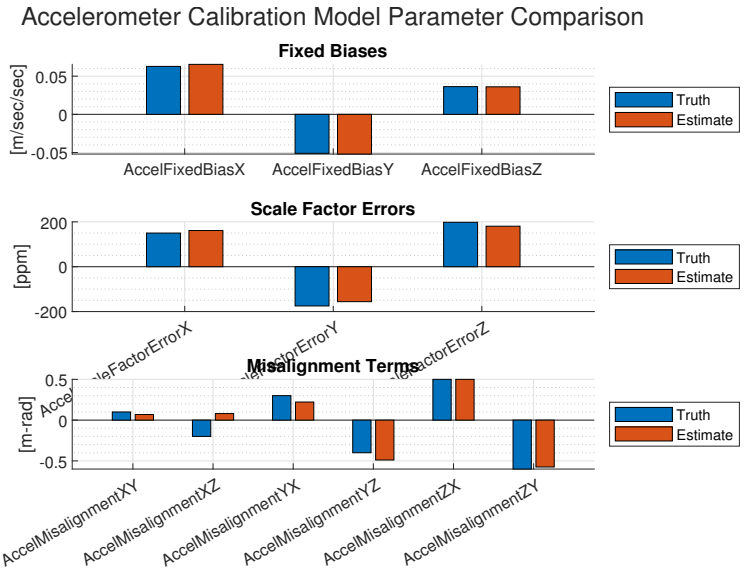

Figure 7: Estimated Accelerometer Model Parameters

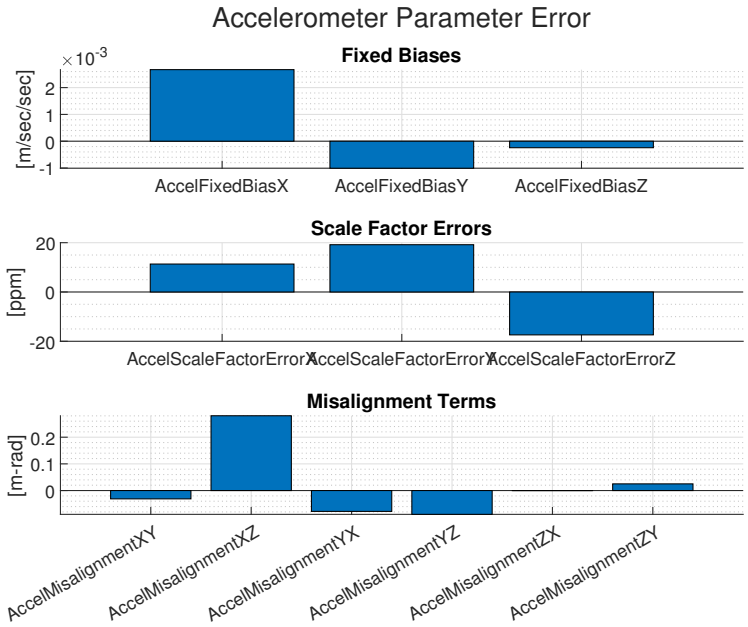

Figure 8: Accelerometer Model Parameter Error

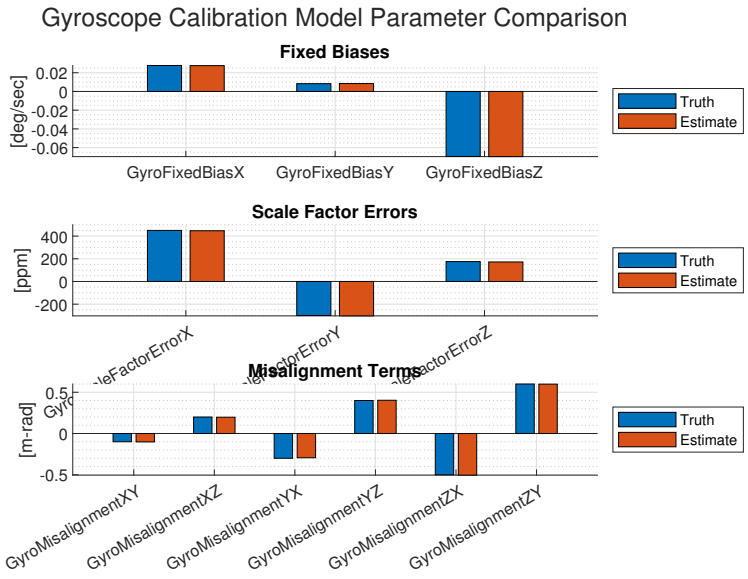

Figure 9: Estimated Gyroscope Model Parameters

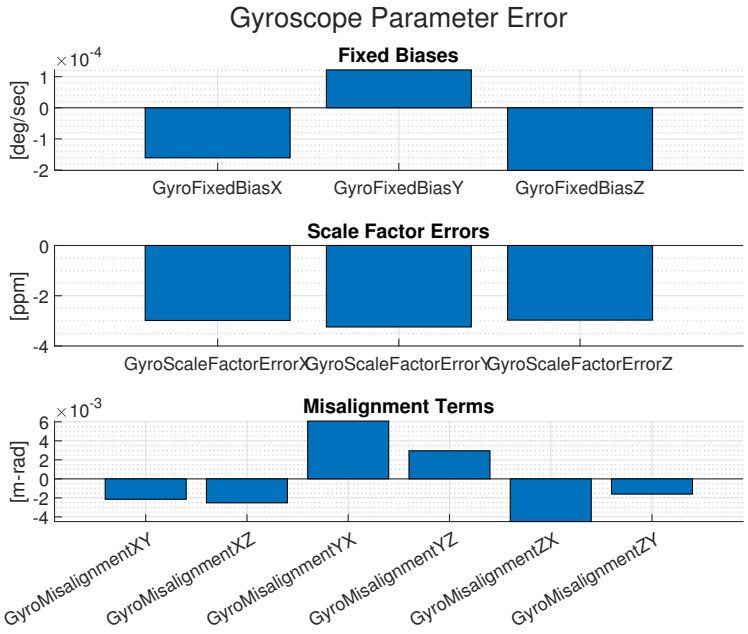

Figure 10: Gyroscope Model Parameter Error

3.2.3 Model Covariance and 95% Confidence Bounds

In preparation for formulating a weighted least squares solution, the weighted matrices were used to compute the model covariance and resulting 95% confidence bounds.

Figure 11: Accelerometer 95% Confidence Bounds

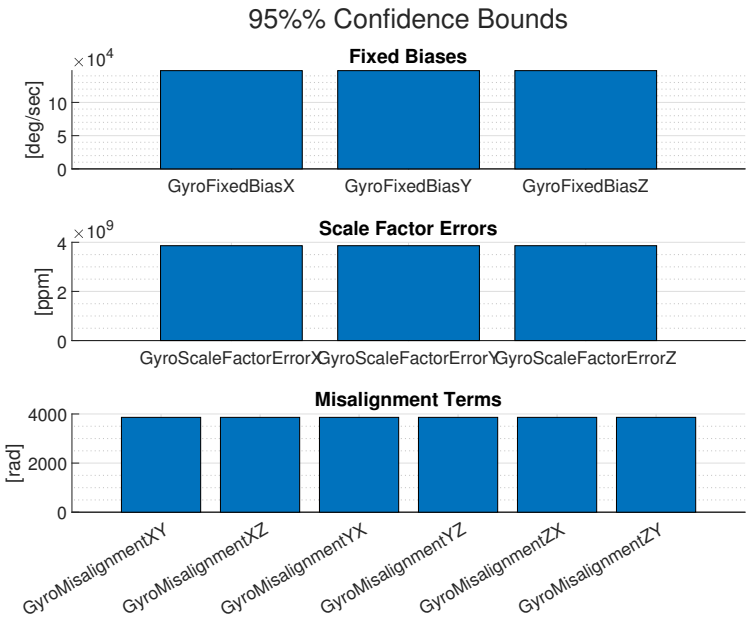

Figure 12: Gyroscope 95% Confidence Bounds

In each case, the confidence bounds are wildly higher than the error actually achieved through the generalized model inverse solution!

3.3 Multi-Axis Motion Calibration Sequence

In response to still lacking full rank with the single-axis motion calibration sequences, yet another calibration sequence was designed to put axis of the UUT in motion at the same time in hopes of establishing model operators of full rank. Figures 13 and 14 show the designed motion profile.

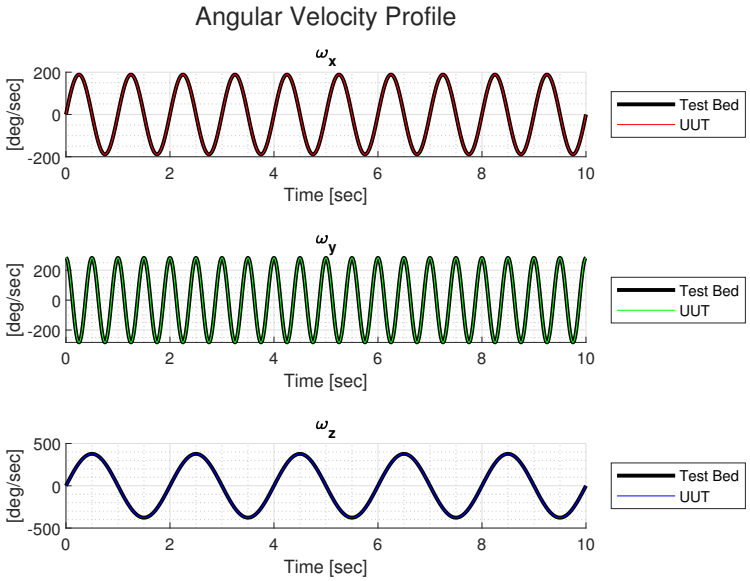

Figure 13: Multi-Axis Angular Velocity Profile

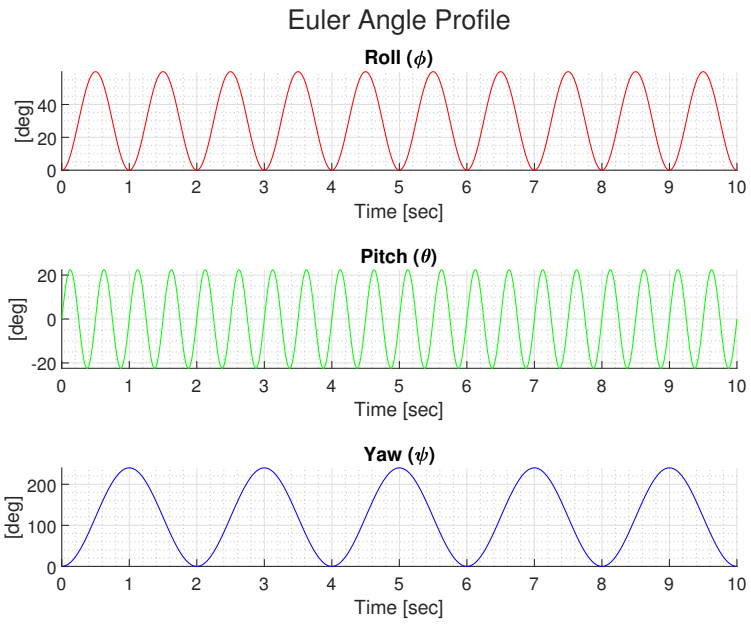

Figure 14: Multi-Axis Euler Angle Profile

Due to the rotations of the test bed, the specific force is also altered as shown in figure 15.

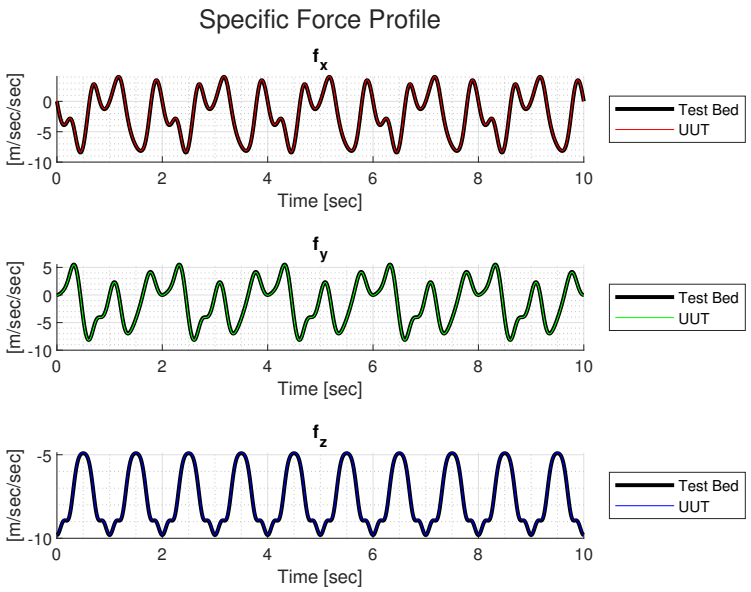

Figure 15: Multi-Axis Specific Force Profile

3.3.1 Model Operator Rank

Even with new motion profiles, both model operators G_a and G_g are not full rank.

$$\begin{aligned} \text{rank}\,(G_a) = 12, \;\; G_a \in \mathbb{R}^{909\times 12} \\ \text{rank}\,(G_g) = 12, \;\; G_g \in \mathbb{R}^{909\times 12} \end{aligned} \tag{19}$$

In response, a model solution was still obtained using the generalized inverse. This rank-deficiency is of the type "$p = n$ and $p < m$, in which the data null space is non-trivial but the model null space is trivial. This implies that the solution will be unique, but cannot fit the general data exactly. For both G_a and G_g, a singular value decomposition (SVD) was performed and each decomposed matrix was truncated to the rank of the matrix. The generalized inverse model was formed accordingly below.

$$\begin{aligned} \boldsymbol{m}_\dagger^a = V_{a,p} S_{a,p}^{-1} U_{a,p}^T \boldsymbol{d}_a \\ \boldsymbol{m}_\dagger^g = V_{g,p} S_{g,p}^{-1} U_{g,p}^T \boldsymbol{d}_g \end{aligned} \tag{20}$$

Each model resolution matrix $R_m = V_p V_p^T$ shows that each model parameter has perfect resolution. The singular values for each model operator are shown in figures 16 and 17.

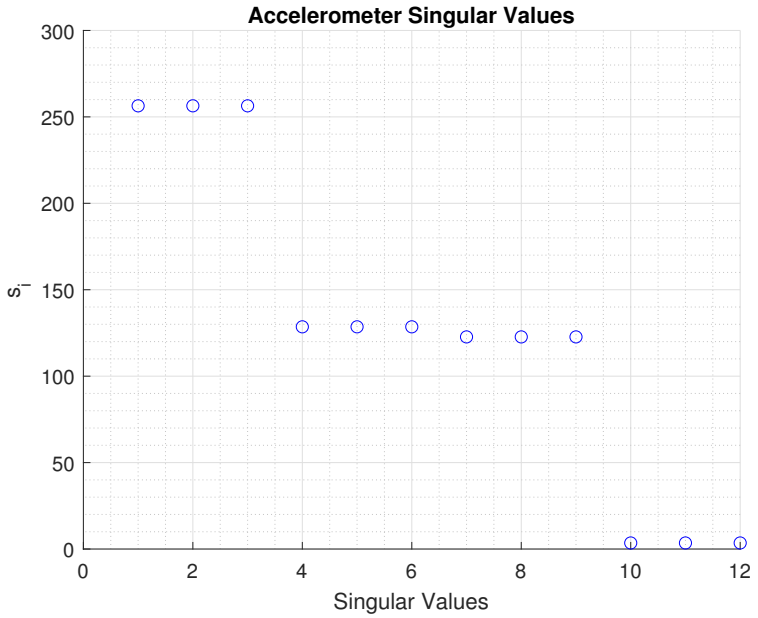

Figure 16: Accelerometer Singular Values

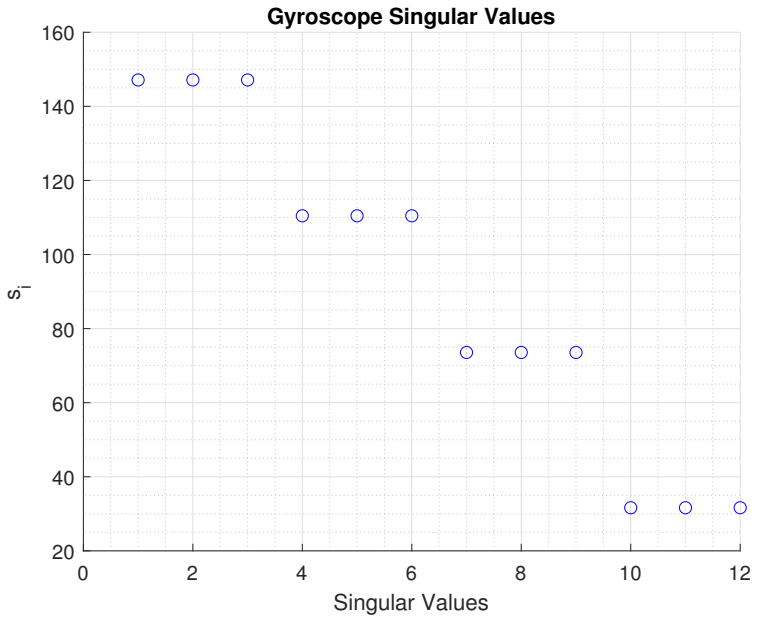

Figure 17: Gyroscope Singular Values

3.3.2 Estimated Model Parameters

The estimated model parameters and their associated errors are provided in figures 18, 19, 20, and 21.

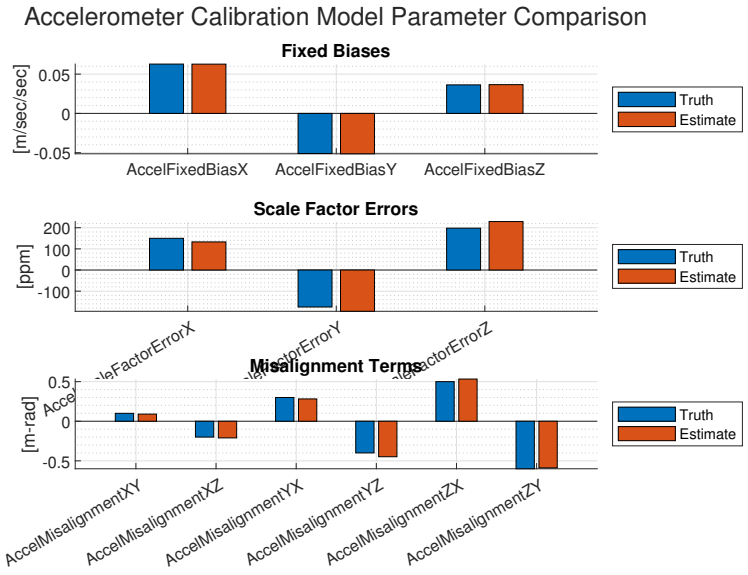

Figure 18: Estimated Accelerometer Model Parameters

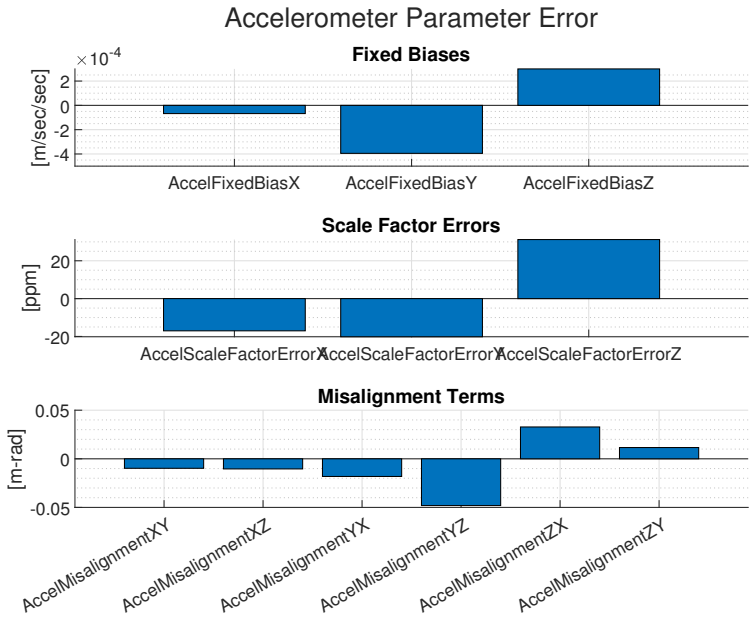

Figure 19: Accelerometer Model Parameter Error

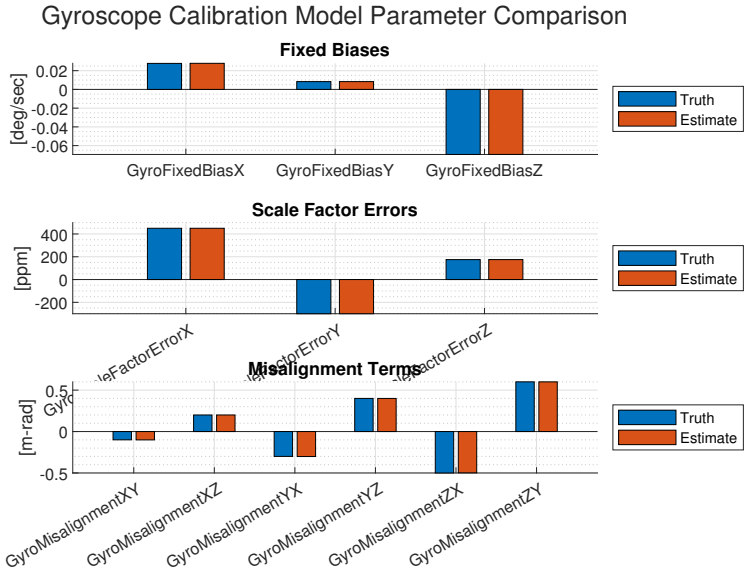

Figure 20: Estimated Gyroscope Model Parameters

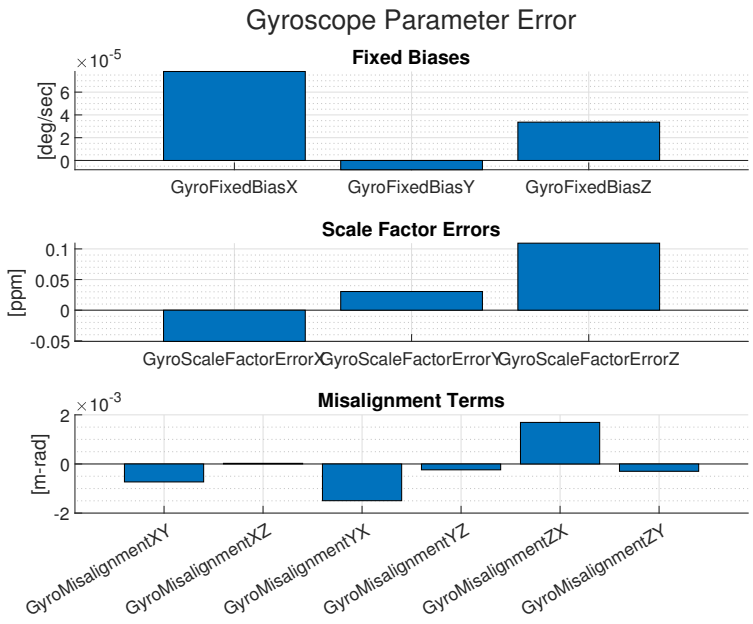

Figure 21: Gyroscope Model Parameter Error

3.3.3 Model Covariance and 95% Confidence Bounds

In preparation for formulating a weighted least squares solution, the weighted matrices were used to compute the model covariance and resulting 95% confidence bounds.

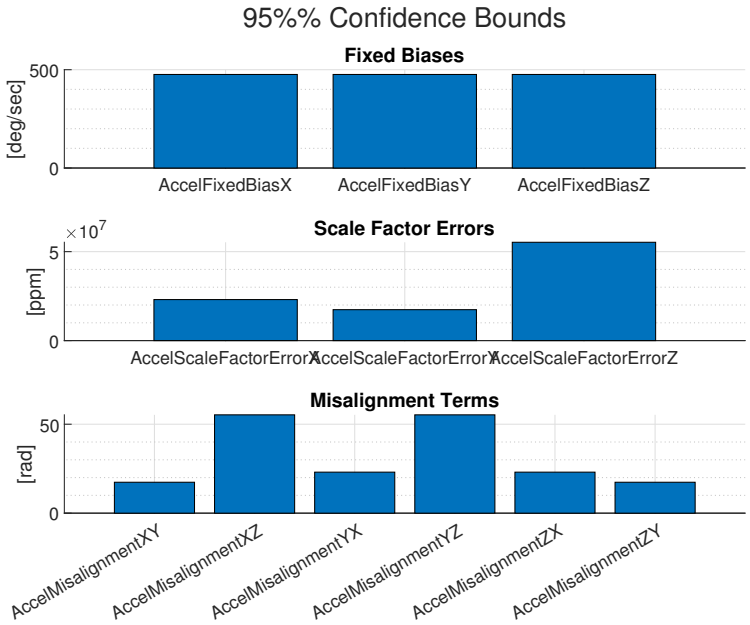

Figure 22: Accelerometer 95% Confidence Bounds

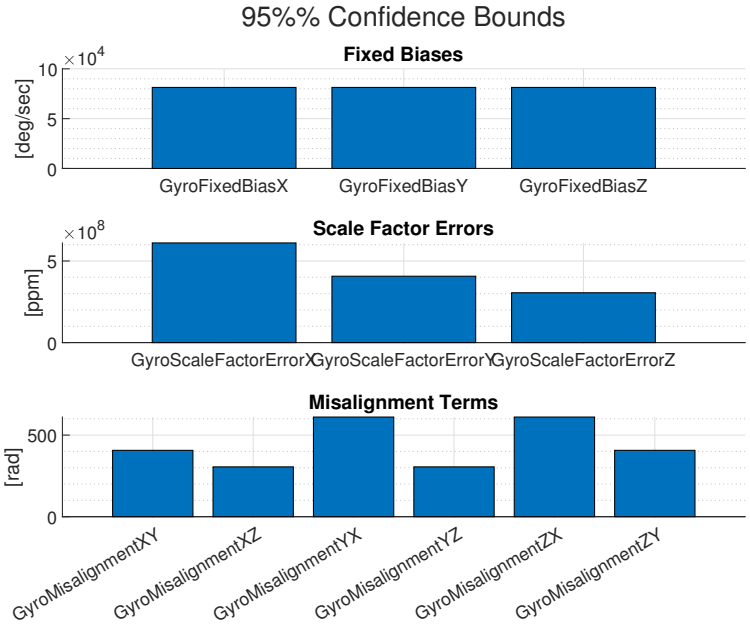

Figure 23: Gyroscope 95% Confidence Bounds

In each case, the confidence bounds are wildly higher than the error actually achieved through the generalized model inverse solution!

4 Discussion

Throughout this project, the biggest surprise was the inability to form a full rank model operator. This results was completely unexpected when the project began. In the first case with the traditional calibration sequence comparison, a rank of six corresponds solely to the fact six different tests were used. Because of this, it was expected that the sinusoidal motion of the calibration sequences would provide a unique observation at each time step. I am still trying to understand why for both the single-axis motion and multi-axis motion cases, why are these model operators only of rank 12? I could use some assistance with this aspect!

One major expected benefit of moving from traditional inertial sensor calibration to systematic inertial sensor calibration was the fact that some measure of uncertainty could be established for each model parameter. It was completely unexpected that the resulting model covariance and 95% confidence bounds are several orders of magnitude above the error achieved by the generalized inverse solution. Perhaps this is related to the fact that the model operator matrices themselves were not full rank. I could really use some help understanding why this is the case, I suspect that something done along the way may not be correct!

Regardless of the inability to achieve a full-rank model operator, the generalized inverse solutions were still able to closely match the true parameters used to generate the data. The residual error in the model parameters are appropriate to be considered "adaquete" for low-stakes navigation such as a hobbyist UAV.

I have some questions about my work that I'll ask here. I'll remove these questions for the final draft of course!

- When I performed the SVD, can I perform this on the weighted model operators, or must the SVD be performed only on the original matrices?
- If performing the SVD on the weighted model operators is permitted, is it still valid to perform the χ^2 test and compute a p-value? If not, then why?
- I am considering trying out a 0^{th} order Tikhonov regularization as well between now and the final draft to see how it compares to the generalized inverse solution. Would you recommend adding this approach?
- I suspect that if I performed a Monte-Carlo experiment to compare against the computed 95% confidence bounds, how does that work when computing the generalized inverse solution? I suppose the answer to this question depends on the answer to the first question.

5 Conclusion

Inertial sensor calibration is an essential activity before installing an IMU into a self-driving vehicle for the purposes of navigation. Traditional calibration methods use simple tests on their respective rotational test beds and post-process the collected data in piece-meal sections to compute only the most basic of IMU error sources. In an effort to improve the status-quo, systematic calibration seeks to leverage batched estimation methods to extend model complexity and make use of all available information to estimate its model parameters. In addition, systematic calibration also establishes some measure of uncertainty for each model parameter which is useful for verifying the final calibration parameters used before vehicle application.

Systematic calibration through the lens of inverse problem techniques provides opportunities to assess the conditioning of the discrete linear inverse problems formed. When comparing the same basic models used in traditional IMU calibration, unexpected difficulty in achieving a full-rank model operator required the use of forming generalized inverse solutions. Also model resolution was preserved in the formation of the solutions, there still remains unanswered questions about the covariance that can be assigned to each model parameter. In the end, the generalized model solutions were still surprisingly close to the true model parameters used in simulation. As a result, the resulting model parameters from the generalized inverse solution are still within an "adaquete" range for low-stakes navigation such as a hobbyist UAV.

References

[1] P. Groves, *Principles of GNSS, Inertial, and Multisensor Integrated Navigation Systems, Second Edition*. GNSS/GPS, Artech House, 2013.

[2] P. G. Savage, "Improved strapdown inertial measurement unit calibration procedures," in *2018 IEEE/ION Position, Location and Navigation Symposium (PLANS)*, pp. 522–533, 2018.

[3] H. Rahimi and A. A. Nikkhah, "Improving the calibration process of inertial measurement unit for marine applications," *NAVIGATION: Journal of the Institute of Navigation*, vol. 67, no. 4, pp. 763–774, 2020.

[4] A. Kozlov and F. Kapralov, "Millimeter-level calibration of imu size effect and its compensation in navigation grade systems," in *2019 DGON Inertial Sensors and Systems (ISS)*, pp. 1–12, 2019.

[5] X. Li, W. Huang, X. Zhu, and Z. Zhao, "Mems-imu error modelling and compensation by 3d turntable with temperature chamber," in *2022 International Symposium on Networks, Computers and Communications (ISNCC)*, pp. 1–5, 2022.

[6] C.-Y. Hung and S.-C. Lee, "A calibration method for six-accelerometer ins," *International Journal of Control Automation and Systems*, vol. 4, 10 2006.

[7] D. L. Olson, J. Bingham, and M. R. Walker, "A generalized imu modeling framework for varying inertial sensing technologies and performance grades," 06 2023.

[8] "Ieee standard specification format guide and test procedure for linear single-axis, nongyroscopic accelerometers," *IEEE Std 1293-2018 (Revision of IEEE Std 1293-1998)*, pp. 1–271, 2019.

[9] "Ieee standard specification format guide and test procedure for coriolis vibratory gyros," *IEEE Std 1431-2004*, pp. 1–78, 2004.

[10] "Ieee standard for specifying and testing single-axis interferometric fiber optic gyros," *IEEE Std 952-2020 (Revision of IEEE Std 952-1997)*, pp. 1–93, 2021.

[11] "Ieee specification format for single-degree-of-freedom spring-restrained rate gyros," *ANSI/IEEE Std 292-1969*, pp. 1–16, 1968.

[12] "Ieee standard specification format guide and test procedure for single-degree-of-freedom rate-integrating gyros," *IEEE Std 517-1974*, pp. 1–60, 1974.

[13] "Ieee standard specification format guide and test procedure for single-axis laser gyros," *IEEE Std 647-2006 (Revision of IEEE Std 647-1995)*, pp. 1–96, 2006.

[14] "Ieee specification format guide and test procedure for two-degree-of-freedom dynamically tuned gyros," *ANSI/IEEE Std 813-1988*, pp. 1–68, 1989.

[15] J. K. Bingham, "Rotational testbed simulator." https://github.com/sandialabs/RTSim, 2024.

[16] Q. Cai, G. Yang, N. Song, and Y. Liu, "Systematic calibration for ultra-high accuracy inertial measurement units," *Sensors*, vol. 16, no. 6, 2016.

[17] Safran, "Stim300 imu non-gps aided inertial measurement unit." https://safran-navigation-timing.com/product/stim300/. Accessed: March 30, 2025.

[18] I. Aerosmith, "2103c series three axis position and rate table system." https://www.ideal-aerosmith.com/wp-content/uploads/2024/02/2102C.pdf. Accessed: March 30, 2025.

6 Appendix

6.1 Traditional IMU Calibration Post-Processing

From equation 2 and collected test data listed in table 1, the accelerometer bias $\boldsymbol{b}_a$ can be solved from the collected test data.

$$\boldsymbol{b}_a = \begin{bmatrix} b_{a,x} \\ b_{a,y} \\ b_{a,z} \end{bmatrix} = \frac{1}{2} \begin{bmatrix} \bar{f}_x^{+\mathrm{x}} + \bar{f}_x^{-\mathrm{x}} \\ \bar{f}_y^{+\mathrm{y}} + \bar{f}_y^{-\mathrm{y}} \\ \bar{f}_z^{+\mathrm{z}} + \bar{f}_z^{-\mathrm{z}} \end{bmatrix} \tag{21}$$

Likewise, accelerometer scale factor terms within the quantity M_a can also be computed, where g is the magnitude of the accelerometer due to gravity at that specific location at the inertial test laboratory.

$$\boldsymbol{s}_a = \begin{bmatrix} s_{a,x} \\ s_{a,y} \\ s_{a,z} \end{bmatrix} = \frac{1}{2g} \begin{bmatrix} \bar{f}_x^{+\mathrm{x}} - \bar{f}_x^{-\mathrm{x}} \\ \bar{f}_y^{+\mathrm{y}} - \bar{f}_y^{-\mathrm{y}} \\ \bar{f}_z^{+\mathrm{z}} - \bar{f}_z^{-\mathrm{z}} \end{bmatrix} - 1 \tag{22}$$

Accelerometer misalignment uses off-axis terms from each collected test where each misalignment term is computed separately.

$$\begin{aligned} m_{a,xy} &= \frac{1}{2g} \left(\bar{f}_x^{+\mathrm{y}} - \bar{f}_x^{-\mathrm{y}} \right) \\ m_{a,xz} &= \frac{1}{2g} \left(\bar{f}_x^{+\mathrm{z}} - \bar{f}_x^{-\mathrm{z}} \right) \\ m_{a,yx} &= \frac{1}{2g} \left(\bar{f}_y^{+\mathrm{x}} - \bar{f}_y^{-\mathrm{x}} \right) \\ m_{a,yz} &= \frac{1}{2g} \left(\bar{f}_y^{+\mathrm{z}} - \bar{f}_y^{-\mathrm{z}} \right) \\ m_{a,zx} &= \frac{1}{2g} \left(\bar{f}_z^{+\mathrm{x}} - \bar{f}_z^{-\mathrm{x}} \right) \\ m_{a,zy} &= \frac{1}{2g} \left(\bar{f}_z^{+\mathrm{y}} - \bar{f}_z^{-\mathrm{y}} \right) \end{aligned} \tag{23}$$

Also from equation 2, the gyroscope bias $\boldsymbol{b}_g$ can be solved from the collected test data.

$$\boldsymbol{b}_g = \begin{bmatrix} b_{a,x} \\ b_{a,y} \\ b_{a,z} \end{bmatrix} = \frac{1}{2} \begin{bmatrix} \bar{\omega}_x^{+\mathrm{x}} + \bar{\omega}_x^{-\mathrm{x}} \\ \bar{\omega}_y^{+\mathrm{y}} + \bar{\omega}_y^{-\mathrm{y}} \\ \bar{\omega}_z^{+\mathrm{z}} + \bar{\omega}_z^{-\mathrm{z}} \end{bmatrix} \tag{24}$$

Gyroscope scale factor terms within the quantity M_g can also be computed, where ω_{test} is the magnitude of the accelerometer due to gravity at that specific location at the inertial test laboratory.

$$\boldsymbol{s}_g = \begin{bmatrix} s_{g,x} \\ s_{g,y} \\ s_{g,z} \end{bmatrix} = \frac{1}{2\omega_{\text{test}}} \begin{bmatrix} \bar{\omega}_x^{+\mathrm{x}} - \bar{\omega}_x^{-\mathrm{x}} \\ \bar{\omega}_y^{+\mathrm{y}} - \bar{\omega}_y^{-\mathrm{y}} \\ \bar{\omega}_z^{+\mathrm{z}} - \bar{\omega}_z^{-\mathrm{z}} \end{bmatrix} - 1 \tag{25}$$

Gyroscope misalignment uses off-axis terms from each collected test where each misalignment term is computed separately.

$$\begin{aligned} m_{g,xy} &= \frac{1}{2\omega_{\text{test}}} \left(\bar{\omega}_x^{+\mathrm{y}} - \bar{\omega}_x^{-\mathrm{y}} \right) \\ m_{g,xz} &= \frac{1}{2\omega_{\text{test}}} \left(\bar{\omega}_x^{+\mathrm{z}} - \bar{\omega}_x^{-\mathrm{z}} \right) \\ m_{g,yx} &= \frac{1}{2\omega_{\text{test}}} \left(\bar{\omega}_y^{+\mathrm{x}} - \bar{\omega}_y^{-\mathrm{x}} \right) \\ m_{g,yz} &= \frac{1}{2\omega_{\text{test}}} \left(\bar{\omega}_y^{+\mathrm{z}} - \bar{\omega}_y^{-\mathrm{z}} \right) \\ m_{g,zx} &= \frac{1}{2\omega_{\text{test}}} \left(\bar{\omega}_z^{+\mathrm{x}} - \bar{\omega}_z^{-\mathrm{x}} \right) \\ m_{g,zy} &= \frac{1}{2\omega_{\text{test}}} \left(\bar{\omega}_z^{+\mathrm{y}} - \bar{\omega}_z^{-\mathrm{y}} \right) \end{aligned} \tag{26}$$